Remote Sens. **2015**, *7*, 5785-5804; doi:10.3390/rs70505785

OPEN ACCESS

remote sensing

ISSN 2072-4292

www.mdpi.com/journal/remotesensing

Article

Spatial Analysis of Wenchuan Earthquake-Damaged Vegetation in the Mountainous Basins and Its Applications

Huaizhen Zhang [1,2,3], Tianhe Chi [1,*], Jianrong Fan [2,†], Kaiheng Hu[2,†] and Ling Peng [1,†]

[1] Institute of Remote Sensing and Digital Earth, Chinese Academy of Sciences, Beijing 100101, China; E-Mails: zhanghz@radi.ac.cn (H.Z.); PL20158@126.com(L.P.)

[2] Institute of Mountain Hazards and Environment, Chinese Academy of Sciences, Chengdu 610041, China; E-Mails: fjrong@imde.ac.cn (J.F.); khhu@imde.ac.cn (K.H.)

[3] University of Chinese Academy of Sciences, Chinese Academy of Sciences, Beijing 100049, China

† These authors contributed equally to this work.

* Author to whom correspondence should be addressed; E-Mail: chith@radi.ac.cn; Tel./Fax: +86-10-6485-2671.

Academic Editors: Richard Gloaguen and Prasad S. Thenkabail

Received: 15 October 2014 / Accepted: 29 April 2015 / Published: 7 May 2015

Abstract: The 2008 Wenchuan Earthquake induced landslides that destroyed large swaths of mountain vegetation. Presently, the damaged vegetation areas are exhibiting various stages of recovery depending on environments. A spatial analysis of earthquake-damaged and recovered vegetation can provide useful information for understanding landslide processes. The mountainous watersheds of the Minjiang River Upstream, near Yinxiu Town (one of the highest seismic intensity zones during the Wenchuan earthquake) were selected. A DSAL (digital elevation model (DEM), slope, aspect and lithology) spatial zonation method was established to detect natural features of the vegetation survival environments, and damaged and recovered vegetation areas were extracted using the normalized difference vegetation index (NDVI) changes form multi-temporal (2001–2014) Landsat Thematic Mapper/Enhanced Thematic Mapper/Operational Land Imager (TM/ETM/OLI) images. Statistical results show that the vegetation growth was mainly controlled by its survival environments, and vegetation has coupling relations with slope stability. Then, the slope stability model was developed through multivariate analysis of earthquake-damaged vegetation and its controlling factors (*i.e.*, topographic environments and material properties). Application to the Mianyuan River and Subao River basins validated the proposed model, showing that monitoring the vegetation (using the remote sensing images)

can be used to assess the slope stability, and model results show what vegetative conditions with its survival environments are susceptible to landslide processes, although the predicted values may be higher than the actual values in the most mountainous basins. Our modeling approach may also be valuable for use in other regions prone to landslide hazards.

Keywords: Wenchuan earthquake; vegetation; remote sensing; landslides

1. Introduction

On 12 May 2008, the Wenchuan Earthquake (seismic magnitude M_w 7.9 according to the United States Geological Survey (USGS)) triggered numerous landslides (approximately 197, 481 according to the data available to Xu *et al.* in 2013) because of the strong ground motion [1–5]. Statistical analyses of the earthquake-induced landslide distributions have been performed, and most of these studies focused on general correlations of landslide occurrences with elevation, slope gradient, aspect, distance from the earthquake source and geologic units [1–9]. These studies found that the majority of earthquake geo-hazards were distributed on slopes of 20° to 50° in river valleys and canyon sections at elevations below 1500 to 2000 m. In addition, thematic maps of these causative factors have been created to assess the landslide hazards. For example, Xu *et al.* (2013) selected the controlling factors (e.g., slope angle, slope aspect, elevation, distance from drainages, distance from roads, distance from main faults, seismic intensity and lithology) for earthquake-triggered landslide susceptibility mapping using the bivariate statistical method, logistic regressions and support vector machine model [7–9]. These studies can provide valuable insights into the characteristics of co-seismic landslides. However, limited studies have focused on earthquake-damaged vegetation.

Presently, only a limited number of studies have focused explicitly on earthquake-damaged vegetation recovery processes in this region. For example, Cui *et al.* (2012) analysed the destruction of vegetation caused by geo-hazards and associated environmental impacts after the earthquake and found that vegetation destruction was distributed along both sides of the rivers within the earthquake zone [10]. Zhang *et al.* (2014) documented the natural recovery of forests after the earthquake and revealed factors that were correlated with successful vegetation recovery, including soil cover and slope [11]. Vegetation helps to stabilise slope materials by improving the resistance of slopes to both surficial erosion and mass wasting [12,13], and vegetation survival environments are correlated with landslide-formational environments [14–17]. Thus, assessments of the spatial distribution of damaged vegetation and its recovery conditions are important for determining susceptible terrain and surface materials to earthquake-induced landslide processes.

The mountainous basins (watersheds) of the Minjiang River near the Yinxiu town were selected to identify and characterise damaged vegetation areas using multi-temporal (2001–2014) remote sensing images. The aims of this paper were to (1) establish the DSAL (digital elevation model (DEM), slope, aspect and lithology) spatial zonation method to characterize the survival environments of vegetation, which were used to discern the relationships between environmental conditions and vegetation growth, (2) establish a model for slope susceptibility, which was developed through multivariate analysis of earthquake-damaged vegetation and its controlling factors (*i.e.*, topographic environments and material properties).

2. Study Area

The study area was upstream of the Minjiang River (103°15′–103°43′E, 31°03′–31°30′N) and primarily located in the town of Yingxiu in southern Wenchuan County, Sichuan Province, China, which is approximately 10 km northwest of Dujiangyan (Figure 1). This area was selected for three reasons. First, it is close to the Wenchuan Earthquake epicentre and was severely affected by the earthquake because of high levels of seismic shaking, which was characterised by seismic intensity XI based on the seismic intensity map produced by the China Earthquake Administration (CEA, 2008) after intensive field work. Second, the area had rich vegetation before the earthquake, which induced catastrophic landslides that damaged large areas of vegetation and provided an unprecedented amount of data for the analysis of earthquake-damaged vegetation. Third, multi-temporal (2001–2014) Landsat Thematic Mapper/Enhanced Thematic Mapper/ Operational Land Imager (TM/ETM/OLI) images are available that can represent the vegetation changes before and after the earthquake.

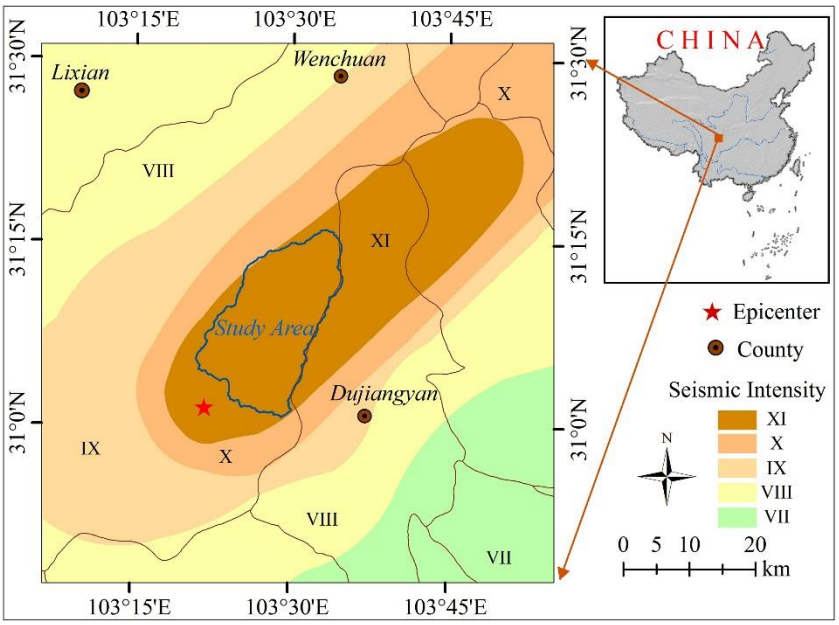

Figure 1. Location of the study area in Sichuan Province, China, and the Wenchuan Earthquake seismic intensity map.

2.1. Topographical and Geological Setting of the Study Area

The study area is characterised by deep rivers and gullies and presents significant variations in the land surface relief (Figure 2a). In addition, active tectonic movements occur in this region because it is located in the fault zones of the Longmenshan Mountains and the Yingxiu-Beichuan fault (the central fault of the Longmenshan thrust belt) runs through the study area [18]. There are approximately 5 types of lithology (granite, diorite, limestone, phyllite and sandstone), with granite rocks dominant in this region (Figure 2b).

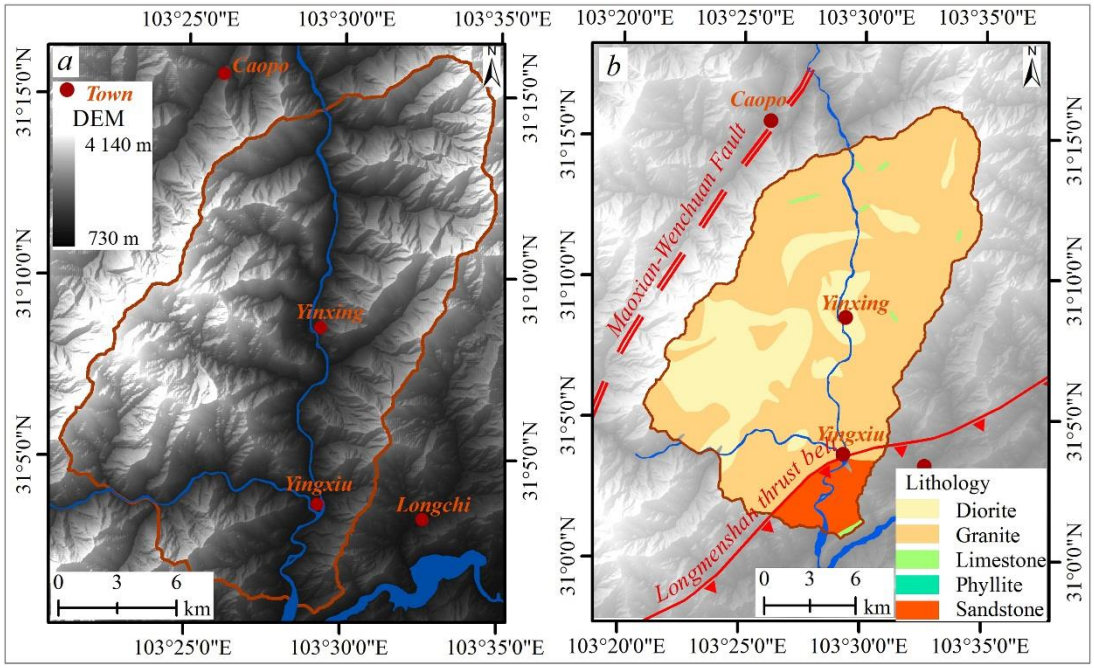

Figure 2. Topographical and geological setting of the study area. (**a**) DEM map of the study area; (**b**) regional geological map and surface rupture zones of the study area.

2.2. Vegetation Changes in the Study Area before and after the Wenchuan Earthquake

This region is influenced by a subtropical moist climate and monsoonal rains that start in early June and continue until September. Mean annual precipitation is approximately 1200 mm, of which about 80% is monsoonal; mean annual temperature is 15.7 °C. As a result of this variable climate, the basin was rich in vegetation before the Wenchuan earthquake (Figure 3a,b). During the earthquake, the earthquake-induced geo-hazards resulted in massive movement of surface material that diminished and destroyed large areas of vegetation (Figure 3c,d). After the earthquake, these damaged vegetation areas began to recovery (Figure 3e). Presently, the areas of damaged vegetation are at various stages of recovery and some have fully recovered within only a few years of the earthquake (Figure 3f).

Remote sensing data operating in the visible, near-infrared, and short-wave infrared portions of the spectrum can provide information on the vegetation dynamics and land cover changes [5,7,8], particularly over large areas or in areas with restricted access [19–21]. The Normalised Difference Vegetation Index (NDVI) is widely used for monitoring, analysing, and mapping temporal and spatial distributions of physiological and biophysical vegetation features. The reported NDVI values significantly responded to changes in vegetation [13–15,22–24].

In the study area, these damaged vegetation areas alter the spectral signatures and NDVI values recorded on remote sensing images. These data sets are derived from both the red and near-infrared spectral bands and are sensitive to changes in biophysical conditions of vegetation, and can therefore be used to detect these damaged vegetation areas.

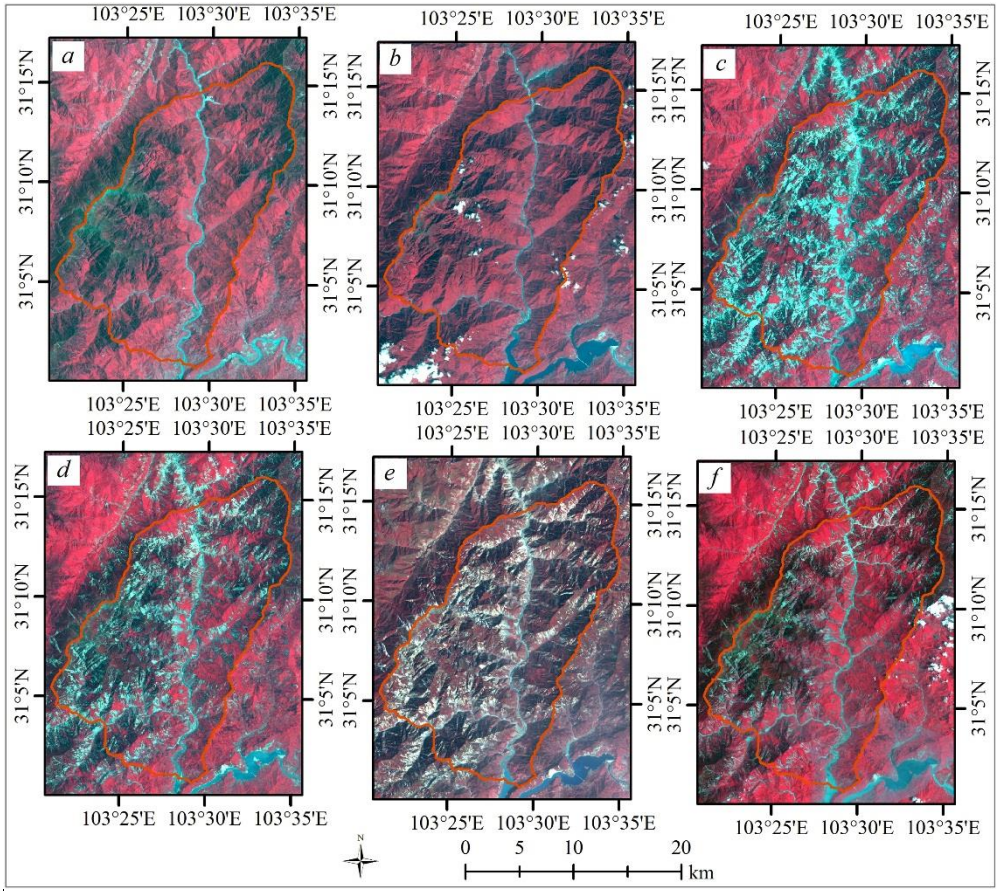

Figure 3. The (**a**) 13 June 2001 Landsat-5 images; (**b**) 18 September 2007 Landsat-5 image; (**c**) 18 July 2008 image; (**d**) 03 June 2009 Landsat-5 image; (**e**) 18 March 2010 Landsat-5 image and (**f**) 1/17 June 2014 Landsat-8 image in the study area.

To detect the change processes of the vegetation conditions, three temporal NDVI images (13 June 2001, 18 July 2008 and 1/17 June 2014) in the vegetation growing season were calculated as shown in Figure 4a–c. These NDVI images indicated that obvious decreases in the NDVI occurred in the damaged vegetation areas, and increases in the NDVI occurred in portions of the damaged vegetation areas where the vegetation had recovered. The per-earthquake vegetation and earthquake-damaged vegetation areas were extracted by examining changes of the NDVI data by examining the pre-earthquake and post-earthquake NDVI images. Figure 4d shows the vegetation distribution before the earthquake, Figure 4e shows the earthquake-damaged vegetation areas during the earthquake, and Figure 4f shows the recovery areas after the earthquake.

The statistical results showed that there was about 332.8 km^2 of vegetation area before the earthquake, and approximately 140.6 km^2 of vegetation area was damaged by earthquakes, with a total area of 350.4 km^2 in the watersheds and approximately 47.1 km^2 remaining unrecovered in 2014. In addition, these damaged vegetation areas during the earthquake account for 12.1% of the total (1160 km^2) Wenchuan-earthquake-triggered landslide area [2].

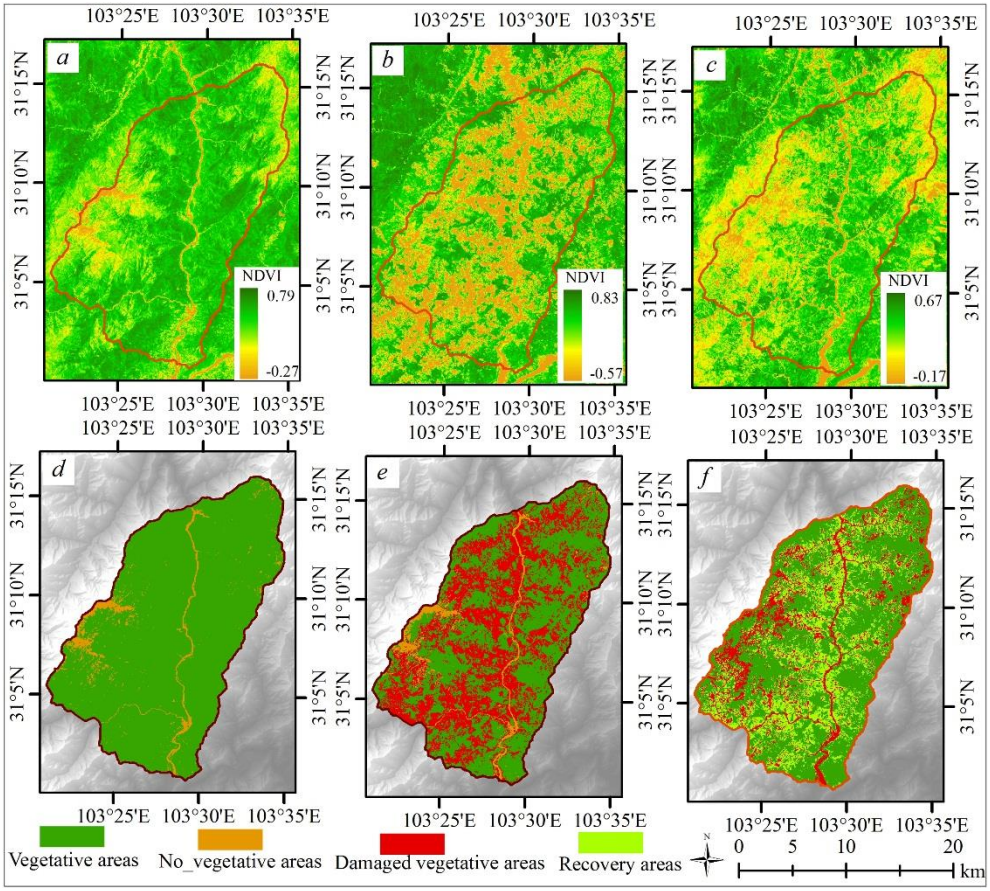

Figure 4. The (**a**) 13 June 2001 NDVI image; (**b**) 18 July 2008NDVI image; (**c**) 1/17 June 2014 NDVI image; (**d**) per-earthquake vegetation map; (**e**) the earthquake-damaged vegetation map; and (**f**) the recovery vegetation map of the study area.

The results also showed differences in the damaged conditions in this region, and the recovery capacity exhibited obvious differences according to area. Because earthquake-damaged vegetation shares an environment with landslide processes and landslide bodies are water and nutrient sources for recovered vegetation, damaged vegetation and its recovery conditions are directly associated with landslide processes. A spatial analysis of earthquake-damaged vegetation and recovered vegetation may provide useful information that can be used to understand landslide processes.

3. Spatial Analysis of the Earthquake-Damaged Vegetation in the Study Area

3.1. DSAL Spatial Zonation for Vegetation Survival Environments

Vegetation growth primarily depends on sunshine, water, temperature and nutrients, and these inputs are directly related to environmental conditions. For example, topography influences vegetation growth in a variety of ways: elevation influences temperature, aspect determines sunshine, and slope affects hydrological conditions. In addition, the geological setting (especially lithology) controls soil properties. River basins represent natural hydrological units for which it is possible to determine balances between the major constituent fluxes of rainfall, evaporation, and river discharge, along with groundwater storage [12]. Additionally, river (gully) basins are a natural result of changes in geomorphic processes. Hence, river

basins can be characterized by their natural features, particularly in terms of topographical environments and vegetation growth.

On the basis of these natural features, the DEM and slope gradient data were mapped into four classes (**1**: $< \mu - \sigma$, **2**: $[\mu - \sigma, \sigma]$, **3**: $[\mu, \mu + \sigma]$, **4**: $> \mu + \sigma$) using the mean (μ) and standard deviation (σ) values. The slope aspect was also divided into four classes (**1**: [45°, 135°], **2**: [135°, 225°], **3**: [225°, 315°], 4: [315°, 360°] and [0°, 45°]) based on the direction of sunshine. Furthermore, lithology units in the basin can be divided into four classes of rock competence based on their lithological and structural properties. The classes include **1**: soft rocks, tertiary and quaternary sediment; **2**: highly fractured and weathered rocks; **3**: folded, inter-bedded limestone and sandstone; **4**: thickly bedded limestone, sandstone, and metamorphic rocks. According to the above considerations, DSAL spatial zonation was defined as one spatial zonation for one given river basin, based on the natural features of the DEM, slope data, aspect data, and lithology conditions. In theory, one river basin can be mapped into 256 DSAL classes.

In the study area, DEM data (Figure 2a) were obtained from a topographic map (scale 1:50,000) with a resolution 25 m, and the slope and aspect were derived from the DEM data. The topographical conditions were found to have natural features. In addition, the study area is primarily comprised of granitic rock (granite and diorite). Then, the study area was zoned spatially using the DSAL zonation method, and the DSAL map was showed in the Figure 5.

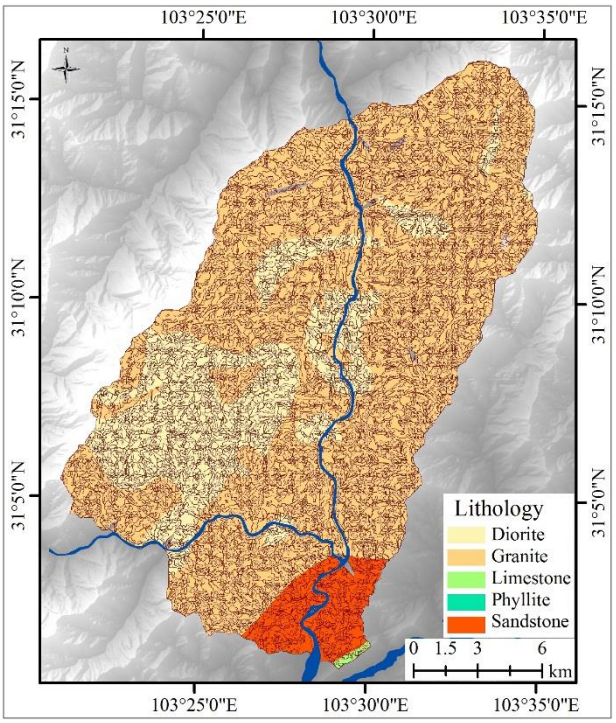

Figure 5. The DSAL (digital elevation model, slope, aspect, and lithology) spatial zonation of the study area.

The results indicate that the basin includes 64 DSAL classes with 8447 DSAL regions; human settlements and water areas had low NDVI values and flat terrain that were extracted separately. Statistical analysis showed that approximately 85% of the units have internal reliefs ranging from 10 to 300 m and approximately 89% of the units have slope gradient changes within 15°. Hence, similar conditions exist in each DSAL region.

3.2. Relationships between Damaged Vegetation and Its Survival Environments in the Study Area

In the study area, earthquake-induced landslides have caused large areas of vegetation damage. Landslide processes are heavily affected by elevation, slope gradient, slope aspect, slope material, and hydrological conditions [14,25–27]. In contrast, vegetation survival conditions are mainly determined by elevation, slope gradient, slope aspect, slope material, and hydrological conditions in the natural environment. Thus, there are several correlations between landslide processes and vegetation growth. Although these complex interactions have not been quantitatively analysed until now, they can be confirmed using statistical analyses or other methods.

To determine the relationships among vegetation (growth conditions), damaged vegetation, recovery vegetation and its survival environments, the topographical conditions (*i.e.*, elevation, slope gradient, slope aspect), lithology conditions and vegetative features (before the earthquake) in each DSAL region were calculated. Also, the vegetation damage probability (*VDP*) was defined as the ratio of damaged vegetation areas to total area in each of the DSAL regions. The vegetation recovery probability (*VRP*) was defined as the ratio of recovered vegetation area to total damaged vegetation area in each of the DSAL regions. Then, statistical relationships among vegetative, *VDP*, *VRP* and its survival environments in the study area are expressed via Equations (1–3).

$$V = 0.678\cos(S) - 0.167D - 0.136\left|\sin(\frac{A}{2} + \frac{\pi}{4})\right|, \quad L = i \tag{1}$$

$$VDP = 1.128\sin(S) - 0.599D - 0.165V\left|\sin(\frac{A}{2} + \frac{\pi}{4})\right|, \quad L = i \tag{2}$$

$$VRP = 0.926\sin(S) - 0.452D + 0.564V\left|\sin(\frac{A}{2} + \frac{\pi}{4})\right|, \quad L = i \tag{3}$$

Here, V is the mean of NDVI values in each of the DSAL regions, S is the mean slope gradient in each of the DSAL regions, D is the ratio of the mean height of the contour above the base (basin mouth) to the total height of the basin, A is the mean slope aspect in each of the DSAL regions, and L is the code for the lithological conditions zonation (i = 4). In addition, Table 1 shows the descriptive statistics and significance values for the model equations.

Table 1. Descriptive statistics and significance values for the model equations.

Equation	Min	Max	Mean	Variance	Standard Deviation	Multiple Correlation Coefficient	Residual Standard Error
Function (1)	0.000	0.825	0.556	0.008	0.072	0.779	0.092
Function (2)	0.000	1.000	0.605	0.005	0.091	0.806	0.174
Function (3)	0.013	0.928	0.605	0.006	0.121	0.712	0.253

All of the above results indicate that the probabilities of vegetation damage and its recovery capacity are both strongly correlated with topographical characteristics. Additionally, these results demonstrate that DSAL spatial zonation is reasonable for detecting the relationships between earthquake-damaged vegetation and survival environments.

3.3. Relationships between Vegetation and Slope Stability

The assemblage of trees and other vegetation that grows above hillslopes plays an important role in intercepting slope materials and protecting them from the actions of sunshine, wind and rain. Vegetation, including plant litter (leaves), helps stabilise the slope materials (1) by extensively altering the soil hydrology by reducing water loss and transpiration, intercepting raindrops and dissipating erosive energy and (2) by altering the mechanical and hydrological properties of the soil by affecting the developing root systems [28–30]. Thus, vegetation improves resistance on slopes to surficial erosion and mass wasting, whereas the removal of slope vegetation tends to accelerate or increase slope failure. Although the impact of vegetation on slope stability in mountainous regions are understood and documented, it is difficult to predict how vegetation will impact mass movement processes, such as landslides and mudflows.

Endo and Tsuruta (1969) determined the reinforcement effect of a root system based on shear strength, and showed that increased strength is directly proportional to root density [28]. Roots are the primary pathway for water and nutrient uptake by plants, and the surface material along the slope creates a root ecosystem conducive to vegetation growth. The nutrient and water inputs, which control vegetation growth, are positively correlated with surface material properties. Meanwhile, surface materials make up the bulk of landslides, and landslide processes are largely determined by the slope gradient, slope materials, elevation, and hydrological conditions. All these causative factors influence vegetation growth and the vegetation survival environment. Thus, there are some coupling relationships between landslides and vegetation, and spatial analysis of landslide-damaged vegetation is important for understanding which terrain and surface materials are susceptible to landslides. Although there is not yet a complete understanding of the interaction of vegetation and landslides, these coupling relationships can be confirmed by the use of statistical analyses or other methods.

3.4. Slope Stability Susceptibility Assessment in the Earthquake-Affected Region

The Wenchuan earthquake triggered many geo-hazards, especially landslides and collapses in the middle and high mountainous areas of China. The reduction of shear strength and overall soil cohesion, combined with ground acceleration from seismic waves, was responsible for the failure of many shallow slopes in the affected region [31]. In essence, the earthquake-induced geo-hazards are strongly controlled by the three most important factors, *i.e.*, topographical conditions, slope material properties, and ground shaking. It is a quite complex process when an earthquake produces a range of ground shaking levels at sites throughout the region, and the ground shaking condition is more difficult to handle in modeling practice. We took into account that earthquake-induced geo-hazards are greatly influenced by topographical conditions and slope material properties at the basin scale, for the study area is located in one of the highest seismic intensity zones (Wenchuan earthquake) and the differences of the landslide occurrence probabilities at different seismic shaking levels are relatively small.

Previous studies in the area affected by the Wenchuan earthquake have demonstrated that earthquake-induced geo-hazards are strongly correlated with elevation, slope gradient and aspect, geological units, distances to the epicenter and active faults, and seismic intensity [1,3–5,8,9]. Our spatial distribution analysis of earthquake-damaged vegetation indicates that the probability of vegetation damage (*VDP*) is influenced by the elevation, slope gradient and aspect, lithology, and vegetative

features of the slope. All of these factors can influence slope failure processes. Thus, Pd can be used as an index of slope stability susceptibility. Because Equation (2) is a multivariable linear regression model, the slope susceptibility (*P*) model in the study is expressed via Equation (4).

$$P = 1.128\sin(s) - 0.599d - 0.165v\left|\sin(\frac{a}{2} + \frac{\pi}{4})\right|, \quad L = i \tag{4}$$

Here, *s* is the slope gradient, *d* is the ratio of the height of the contour above the base (basin mouth) to the total height of the basin, *v* is the NDVI value, *a* is the slope aspect value, and *L* is the code for lithological zonation. All of these variables can be obtained from thematic maps representing the various factors (e.g., elevation, slope, aspect, lithology, and NDVI). These data were used to create a map of pre-earthquake slope stability susceptibility in the study area (Figure 6).

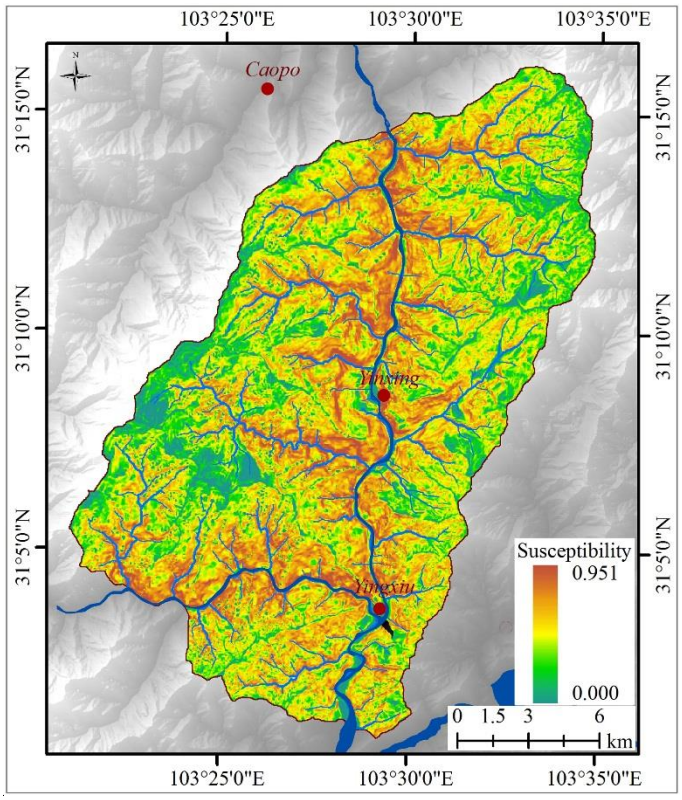

Figure 6. The predicted slope stability susceptibility in the study area.

The model results show that high-susceptibility areas were located along the steep slopes of main streams. Comparing the earthquake-damaged vegetation map (Figure 4e), the results also show good agreement between predicted susceptibility and actual conditions, except for mountaintop areas and some deep-seated landslide areas.

The model provides a time-varying estimate of the slope stability, by linking vegetation growth data with spatially varying topographical environments and materials properties. Also, the remote sensing images are used to monitor the vegetation over time and to assess the slope stability. In addition, the recovery capacity of damaged vegetation is strongly influenced by its survival environments [32] and the landslides that occurred. Hence, monitoring the recovery conditions of damaged vegetation can provide useful information about the landslide processes that occurred.

4. Application

4.1. The Conditions of the Mianyuan River and Subao River

The Mianyuan River (31°26′–31°42′N, 103°54′–104°11′E) is located in the upstream reaches of the Mianyuan River watershed, in Mianzhu County. The 2008 Wenchuan earthquake generated high levels of ground shaking (seismic intensity X) in Mianyuan River basin (Figure 7). The watershed ranges from 669 to 4417 m in elevation and has an area of approximately 411 km^2. The Subao River basin (31°44′–31°50′N, 104°16′–104°26′E) is located in the northeastern part of Beichuan County, and covers an area of approximately 72.6 km^2, with seismic intensity XI during the earthquake (Figure 7). The main topographic features are an elevation range from 720 to 2340 m (mean elevation 1499 m) and a slope range from 0° to 75° (mean angle 30.5°).

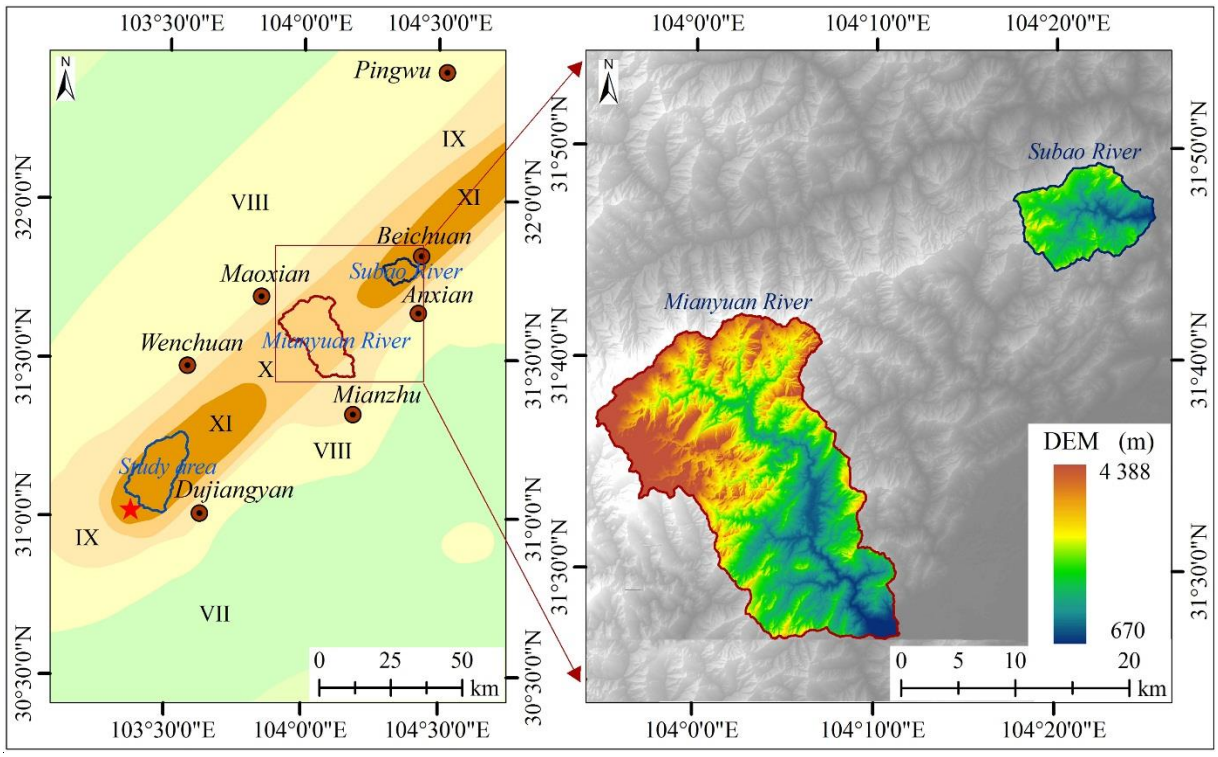

Figure 7. The location of the Mianyuan River and Subao River in the Wenchuan earthquake-affected area and digital elevation (DEM) data.

Mianyuan River is influenced by a subtropical moist climate and monsoonal rains that start in early June and continue until September. The river was rich in vegetation before the earthquake (Figure 8a). During the earthquake, the earthquake-induced geo-hazards that resulted in massive movement of surface material that diminished and destroyed large areas of vegetation (Figure 8b). Statistical results show that the total size of the damaged area was about 101.4 km^2, which accounts for 24.7% of the total area.

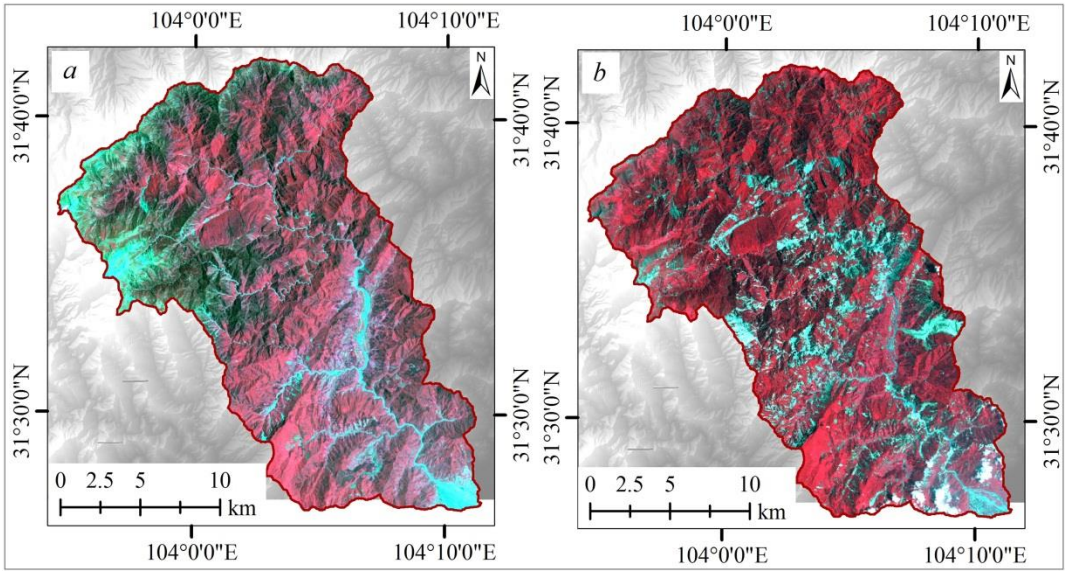

Figure 8. The (**a**) 13 May 2001 Landsat-7 image and (**b**) 18 July 2008 Landsat-5 image in the Mianyuan River.

The Subao River basin is under the influence of a humid subtropical monsoon climate, which is warm and wet. The basin was well covered by forests and shrubs prior to the earthquake (Figure 9a). The earthquake struck the Subao River basin, and the earthquake triggered many landslides that destroyed large areas of vegetation (Figure 9b). Results shows that the damaged vegetation areas are zonally distributed along the rivers and streams, covering an area of 10.1 km^2, which accounts for 13.9% of the total basin area.

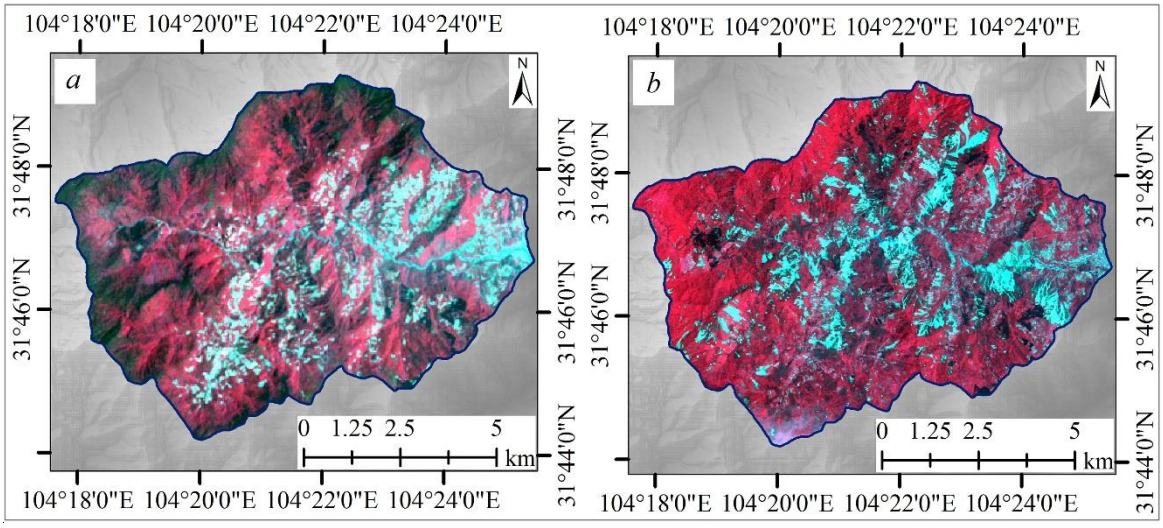

Figure 9. The (**a**) 13 May 2001 Landsat-7 image and (**b**) 4 June 2008 ALOS image in the Subao River.

4.2. The Assessment of Slope Stability Susceptibility in the Mianyuan River and Subao River

The rocks of the Mianyuan River basin primarily consist of Sinian sandstone and siltstone; Cambrian sandstone, siltstone, and slate; Silurian phyllite, schist, and slate; Devonian dolomite limestone and sandstone; carboniferous limestone; Permian limestone and shale; Triassic sandstone, dolomite, limestone,

siltstone, and shale; quaternary deposits; and magmatic rocks, granite, and diorite. Rocks in the Subao River include eight types: dolomite and dolomitic limestone; siltite and quartz sandstone; limestone intercalated with phyllite, sandstone; marlite and limestone; phyllite intercalated with limestone; limestone, shale, and sandstone; shale and sandstone; and gravel sand and siltite. Above all, the rocks in the Mianyuan River can be divided into four classes, and the rocks in the Subao River can be divided into three classes.

The slope gradient and slope aspect data can be calculated from the DEM data (Figure 7), and the per-earthquake NDVI data can be calculated from the remote sensing images (Figures 8a and 9a). Then, the slope stability susceptibility maps of the Mianyuan River and Subao River can be calculated using Equation (4), and are shown in the Figure 10.

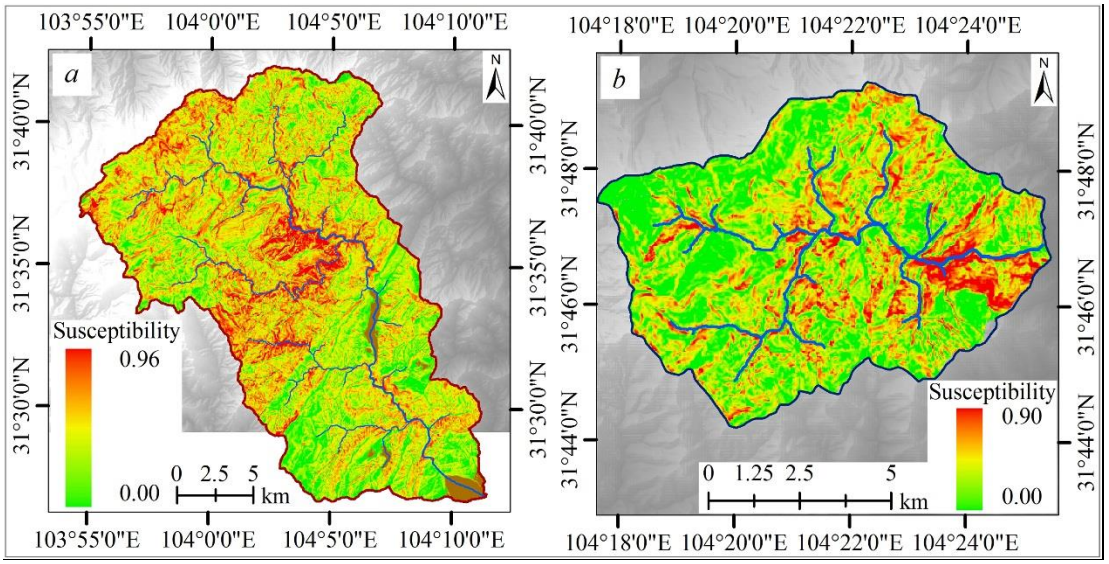

Figure 10. The (**a**) Mianyuan River and (**b**) Subao River predicted slope stability susceptibility maps.

4.3. Results Analysis

The areas of damaged vegetation during the earthquake in the Mianyuan River and Subao River basins were used to verify the predicted slope stability susceptibility map. To assess the accuracy of the proposed method, the predicted slope stability susceptibilities were divided into ten levels, and the damaged vegetation areas in each level were calculated and were shown in the Table 2. Table 2 shows the total area (*TA*, km^2), damaged vegetation area (*DA*, km^2) and damaged probability (*DP*, %) in each susceptibility level. Results indicate that the *DP* values displays a relatively positive correlation with the susceptibility level in both Mianyuan River and Subao River, although the *DP* values are lower than the mean predicted values in each level. Statistical results show that the *VDP* values in Mianyuan River and Subao River are 0.247 and 0.139, these values are far below *VDP* (0.422) in the study area.

The Mianyuan River is located in the region with seismic intensities of X during the earthquake, while the earthquake generated high levels of ground shaking (seismic intensity XI) in the Subao River, though the Subao River area is far from the epicenter. We find that the differences in shaking conditions during the earthquake make the *DP* values lower than the predicted values.

Table 2. Statistical results of the damaged vegetation areas in the Mianyuan and Subao Rivers.

Susceptibility Level	Mianyuan River (km^2)			Subao River (km^2)		
	TA	*DA*	*DP* (%)	*TA*	*DA*	*DP* (%)
1: 0.0~0.1	65.04	5.96	9.2	27.54	1.39	5.1
2: 0.1~0.2	47.89	5.40	11.3	15.19	1.29	8.5
3: 0.2~0.3	69.78	12.72	18.2	14.06	2.28	16.2
4: 0.3~0.4	83.28	20.44	24.5	9.13	2.41	26.4
5: 0.4~0.5	70.11	21.35	30.5	3.97	1.26	31.6
6: 0.5~0.6	43.03	17.18	39.9	1.25	0.56	44.7
7: 0.6~0.7	19.68	10.16	51.6	0.68	0.38	55.4
8: 0.7~0.8	8.40	5.49	65.4	0.44	0.29	66.3
9: 0.8~0.9	2.70	1.90	70.4	0.29	0.23	78.3
10: 0.9~1.0	0.97	0.78	80.7	/	/	/

The above results indicate that the quantitative slope stability susceptibility should be regarded as providing a general assessment of slope stability (landslide) susceptibility rather than the precise probability of landslide occurrence, owing to the complexity of the landslide processes. Actually, the predicted slope stability susceptibility is used to detect what areas are susceptible to landslide, and the model results cannot predict the actual probability of landslide occurrence during one given earthquake.

5. Discussion

5.1. Shake Map Analysis in the Earthquake-Damaged Vegetation Areas

The peak ground acceleration (PGA) and peak ground velocity (PGV) are two important input parameters for earthquake engineering. Figure 11 shows the shake maps of all study river basins [33].

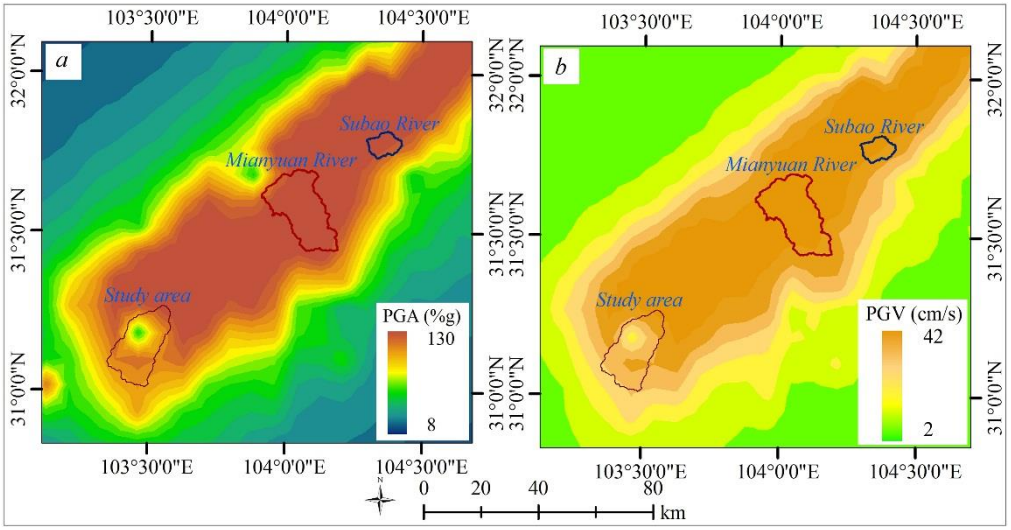

Figure 11. USGS shake maps (Eastern Sichuan, China) of the study area, Mianyuan River and Subao River. (**a**) Peak ground acceleration (PGA, %g) map; (**b**) peak ground velocity (PGV, cm/s) map.

The PGA map (Figure 11a) indicates that both the Mianyuan River and Subao River had high PGA values, and the PGA values in the study area indicated obvious changes. The PGV map (Figure 11b) shows that both the Mianyuan River and Subao River had high PGV values and the study area had low PGV values with obvious changes. All of the results indicated that there were obvious differences between the study area, Mianyuan River and Subao River in the ground motion conditions.

The total areas (*TA*, km^2), damaged vegetation areas (*DA*, km^2) and damaged vegetation probabilities (*DP*, %) with PGA conditions in the study area, Mianyuan River and Subao River are shown in Table 3. The results showed that there were no obvious correlations between the *DP* values and PGA condition, and the study area has obviously high *DP* values than both Mianyuan River and Subao River in most of PGA conditions. Thus, these results can explain why the predicted values are higher than the actual vegetation damaged probability in both Mianyuan River and Subao River.

Table 3. Statistical results of PGA features and its damaged vegetation areas in the study area, Mianyuan River and Subao River.

PGA Level	Study Area (km^2)			Mianyuan River (km^2)			Subao River (km^2)		
	TA	***DA***	***DP* (%)**	***TA***	***DA***	***DP* (%)**	***TA***	***DA***	***DP* (%)**
1: <52	26.69	14.48	54.3	/	/	/	/	/	/
2: 52~56	18.69	10.79	57.7	/	/	/	/	/	/
3: 56~60	23.62	10.22	43.3	/	/	/	/	/	/
4: 60~64	27.34	9.08	33.2	/	/	/	/	/	/
5: 64~68	48.96	18.68	38.2	/	/	/	/	/	/
6: 68~72	124.31	46.73	37.6	2.62	2.24	85.5	1.44	0.04	2.6
7: 72~76	61.20	25.03	40.9	8.89	4.39	49.4	16.75	1.91	11.4
8: 76~80	10.80	3.65	33.8	27.04	4.32	16.0	24.72	4.14	16.8
9: 80~84	9.36	1.91	20.4	68.50	13.50	19.7	21.45	3.91	18.2
10: 84~88	/	/	/	305.64	76.40	25.0	8.25	0.27	3.3
11: >88	/	/	/	/	/	/	0.21	0.00	1.4

Actually, the slope failure (landslide) processes during the earthquakes are very complex processes, and these earthquake-induced landslide occurrences are mainly controlled by the landslide-forming environments and ground shaking conditions during the earthquake. Although the probability of a landslide depends on both forming environments and ground shaking conditions, the latter possess a temporal distribution (it is hard to predict the shaking conditions for the future earthquake) which is more difficult to handle in modelling practice. Therefore, for the landslide assessment, landslide susceptibility mapping is often conducted, in which the extrinsic variables (*i.e.*, rainfall, earthquakes) are not considered in determining the probability of the landslide occurrence [34].

The slope stability in this research was modelled for detecting what areas are susceptible to landslides, and the application demonstrated that the predicted values can provide important information for understanding what terrain and surface materials are susceptible to landslide processes. The application also indicated that the shaking conditions should be considered in determining the (actual) probability of landslide occurrence during one given earthquake, because the ground shaking experienced at one location is a key factor for in earthquake-induced landslides.

5.2. Survival Environments Analysis in the Earthquake-Damaged Vegetation Areas

The spatial distribution of the earthquake-damaged vegetation and its recovery conditions is analyzed statistically to determine how the damaged vegetation and its recovery processes correlate with the topographical environments, pre-earthquake vegetation conditions, and lithology. Firstly, the recovery conditions of these damaged vegetation areas, with a total area of about 834 km^2 (including the study area, Mianyuan River and Subao River), were interpreted using the 1 June 2014 and 17 June 2014 Landsat-8 OLI images. Then, the study area, Mianyan River and Subao River, were mapped into different levels based on the DEM and slope gradient data. Table 4 shows the damaged vegetation areas (*DA*, km^2), the recovered vegetation areas (*RA*, km^2) and pre-earthquake NDVI values (*V*), and slope stability susceptibility values (*p*, %) of each elevation level in the study area, the Mianyan River and Subao River, respectively. Statistical results indicate that about 65.2% of the damaged vegetation areas and about 77.1% of the recovered vegetation areas are distributed at elevations of 1000 to 2250 m, and both the *V* and *p* values in these elevation levels are higher than in other elevation levels.

Table 4. Statistical features of each elevation level in the study area, the Mianyuan River and Subao River.

Elevation	Study Area (km^2)				Mianyuan River				Subao River			
Level (km)	*DA*	*RA*	*V*	*p* (%)	*DA*	*RA*	*V*	*p* (%)	*DA*	*RA*	*V*	*p* (%)
1: <1.00	4.24	2.24	0.52	29.7	6.78	3.67	0.53	35.2	0.68	0.53	0.45	22.1
2: 1.00~1.25	16.01	12.62	0.59	49.8	12.69	8.49	0.57	45.3	2.03	1.75	0.51	33.5
3: 1.25~1.50	20.75	17.18	0.62	51.2	15.18	10.37	0.60	48.1	3.86	3.21	0.53	38.9
4: 1.50~1.75	21.60	17.26	0.63	49.8	12.93	7.71	0.61	50.6	2.17	2.02	0.56	44.8
5: 1.75~2.00	20.18	14.77	0.63	45.8	9.84	5.05	0.62	54.6	0.92	0.67	0.50	23.1
6: 2.00~2.25	17.35	11.78	0.63	42.3	8.45	3.34	0.63	41.3	0.35	0.22	0.46	12.9
7: 2.25~2.50	14.30	8.27	0.61	38.5	6.73	2.57	0.60	33.3	0.16	0.09	0.40	11.7
8: 2.50~2.75	10.42	4.76	0.55	34.2	6.94	1.77	0.54	31.2	/	/	/	/
9: 2.75~3.00	7.88	2.68	0.50	32.1	5.29	0.70	0.49	28.1	/	/	/	/
10: >3.00	7.82	1.98	0.41	22.6	16.47	5.45	0.45	19.2	/	/	/	/

Table 5 shows the *DA*, *RA*, *V*, and *p* values at each slope level in the study area, the Mianyan River and Subao River. Statistical results indicate that about 82.1% of the damaged vegetation areas and about 84.5% of the recovered vegetation areas were distributed at slopes of 25° to 55°. The *V* values have no obvious features, while the *p* values have obvious positive correlation with the slope levels.

Then, the *DA*, *RA*, *V*, and *p* values at each slope aspect zonation and lithology condition in the study area, Mianyan River and Subao River, were calculated, too. However, statistical results indicate that there are no obvious features among these values, since suitable climatic conditions (*i.e.*, plentiful rainfall, warm temperate) enhance recovery capacity and weaken the influences of slope aspect and lithology conditions on the recovery processes in the study area, the Mianyuan River and Subao River.

The above results demonstrate that elevation and slope are the main variables in the survival environments of vegetation. According to the damaged vegetation and its recovery data, about 78.1% of the high-susceptibility areas ($p \geq 0.50$) were distributed at slopes of 25° to 55° and elevations of 1000 to 2250 m, of which the actual mean *VDP* of these areas is 0.72, and the mean NDVI value of the damaged

vegetation areas is about 0.58. Accordingly, the areas with slopes of 25° to 55° and elevations of 1000 to 2250 m can be called "susceptible areas." Statistical results also indicate that there are about 172 km^2 damaged vegetation areas in these susceptible areas, accounting for 68.3% of the total damaged vegetation area.

Table 5. Statistical features of each slope level in the study area, the Mianyuan River and Subao River.

Slope	Study Area (km^2)				Mianyuan River				Subao River			
Level (°)	*DA*	*RA*	*V*	*p* (%)	*DA*	*RA*	*V*	*p* (%)	*DA*	*RA*	*V*	*p* (%)
1: < 15	4.42	1.81	0.52	7.5	2.94	1.33	0.52	10.2	0.74	0.69	0.51	12.3
2: 15~25	5.91	3.43	0.59	17.9	7.03	3.67	0.57	27.3	1.06	0.92	0.56	26.3
3: 25~35	19.04	13.33	0.62	30.5	20.54	10.00	0.58	37.5	1.89	1.68	0.58	35.6
4: 35~45	55.40	39.92	0.63	42.8	34.19	18.73	0.56	48.3	3.24	2.63	0.55	43.1
5: 45~55	43.45	28.20	0.63	54.3	27.01	11.39	0.55	57.9	2.13	1.81	0.52	56.3
6: > 55	12.34	6.84	0.63	63.8	9.58	3.99	0.51	75.2	1.03	0.73	0.47	67.2

Moreover, the statistical results also indicate that these susceptible areas with high NDVI values (NDVI $\geq$ 0.55) have stronger recovery capacity (*VRP* is about 0.82) than other regions (*VRP* is about 0.62), and the damaged vegetation areas with low *p* values have relatively weak recovery capacity. It is believed that these landslide processes determine the damaged conditions of the survival environments and influence recovery processes. In addition, the results also show that good survival environments have high NDVI values before the earthquake, and have strong recovery capacity, too.

5.3. The Validity of the Slope Stability Model

The slope stability model was developed using the earthquake-damaged vegetation data in the mountainous basins of the Wenchuan earthquake-affected region. Hence, the model is suitable for most vegetation-covered mountainous basins of an earthquake-affected region. Applications of the model demonstrated that the model is feasible and the results are reliable. However, we note that the predicted susceptible areas are more useful than the predicted values, and these predicted values are significantly greater than the actual vegetation damage probability in most of the earthquake-hit areas.

In other regions, we can develop a similar model. However, the new model requires sufficient earthquake-damaged vegetation data that includes all possible conditions because the quality of the (existing) damaged vegetation data controls the model accuracy and applicability. In addition, either the selected study area should have similar ground shaking conditions during earthquakes, or the conditions of the earthquake-damaged vegetation areas should be insensitive to the shaking conditions.

6. Conclusions

A DSAL (digital elevation model (DEM), slope, aspect and lithology) spatial zonation method and normalized difference vegetation index (NDVI) changes map derived from multi-temporal (2001–2014) Landsat Thematic Mapper/Enhanced Thematic Mapper/Operational Land Imager (TM/ETM/OLI) images were utilized to detect natural features of the vegetation survival environments, and the damaged and recovered vegetation areas after the 2008 Wenchuan earthquake, respectively.

The method clarified that the vegetation growth has quantitative relationships with its survival environments (*i.e.*, elevation, slope gradient, aspect and lithology conditions) in one given mountain basin; specifically, (1) the slope stability has direct relationships with the topographical environments and pre-earthquake vegetation conditions; (2) the recovery processes and speed of the damaged vegetation areas depend on their survival environments and the type and size of suffered landslides. Therefore, one slope stability model considering NDVI was developed to detect what terrain and vegetation conditions are susceptible to landslide processes. Model results indicated that areas with slopes of 25° to 55°, elevations of 1000 to 2250 m and NDVI $\geq$ 0.55 were susceptible to landslide processes during earthquakes.

The model demonstrated a temporal estimation of slope stability and its effects on vegetation recovery. Monitoring the recovery processes of these damaged vegetation areas indicated that the survival environments (mainly including elevation, and slope gradient) are the main factors which controlled post-earthquake recovery capacity. In addition, most of the damaged areas with pre-earthquake NDVI $\geq$ 0.55 had obviously strong recovery capacity. Although some damaged vegetation areas recovered within a few years after the earthquake, there remains potential for future slope instability. These findings proved that multi-temporal remote sensing images were effective in monitoring the damaged vegetation recovery process over a large mountain area. Higher temporal resolution (*i.e.*, seasonal frequency) images should be investigated in future studies for more detailed vegetation recovery process assessment.

Acknowledgments

This research was financially supported by the National Science and Technology Support Program (No: 2012BAC06B02), Key Projects of the Chinese Academy of Sciences (No: KZZD-EW-05-01-04), and the Beijing Natural Science Foundation (No: 4144088).

Author Contributions

The analysis was performed by Huaizhen Zhang. All authors contributed concepts and participated in discussing and writing the manuscript.

Conflicts of Interest

The authors declare no conflict of interest.

References

1. Huang, R.; Li, W. Development and distribution of geohazards triggered by the 5.12 Wenchuan earthquake in China. *Sci. China Seri. E Technol. Sci.* **2009**, *52*, 810–819.
2. Xu, C.; Xu, X.; Yao, X.; Dai, F. Three (nearly) complete inventories of landslides triggered by the May 12, 2008 Wenchuan mw 7.9 earthquake of China and their spatial distribution statistical analysis. *Landslides* **2013**, *11*, 441–461.
3. Qi, S.; Xu, Q.; Lan, H.; Zhang, B.; Liu, J. Spatial distribution analysis of landslides triggered by 2008.5.12 Wenchuan earthquake, China. *Eng. Geol.* **2010**, *116*, 95–108.

4. Cui, P.; Chen, X.; Zhu, Y.; Su, F.; Wei, F.; Han, Y.; Liu, H.; Zhuang, J. The Wenchuan earthquake (May 12, 2008), Sichuan province, China, and resulting geohazards. *Nat. Hazards* **2009**, *56*, 19–36.
5. Dai, F.C.; Xu, C.; Yao, X.; Xu, L.; Tu, X.B.; Gong, Q.M. Spatial distribution of landslides triggered by the 2008 ms 8.0 Wenchuan earthquake, China. *J. Asian Earth Sci.* **2011**, *40*, 883–895.
6. Xu, C. Preparation of earthquake-triggered landslide inventory maps using remote sensing and GIS technologies: Principles and case studies. *Geosci. Front.* **2014**, doi:10.1016/j.gsf.2014.03.004.
7. Xu, C.; Dai, F.; Xu, X.; Lee, Y.H. Gis-based support vector machine modeling of earthquake-triggered landslide susceptibility in the Jianjiang river watershed, China. *Geomorphology* **2012**, *145–146*, 70–80.
8. Xu, C.; Xu, X.; Dai, F.; Wu, Z.; He, H.; Shi, F.; Wu, X.; Xu, S. Application of an incomplete landslide inventory, logistic regression model and its validation for landslide susceptibility mapping related to the May 12, 2008 Wenchuan earthquake of China. *Nat. Hazards* **2013**, *68*, 883–900.
9. Xu, C.; Xu, X.; Yao, Q.; Wang, Y. GIS-based bivariate statistical modelling for earthquake-triggered landslides susceptibility mapping related to the 2008 Wenchuan earthquake, China. *Q. J. Eng. Geol. Hydrogeol.* **2013**, *46*, 221–236.
10. Cui, P.; Lin, Y.; Chen, C. Destruction of vegetation due to geo-hazards and its environmental impacts in the Wenchuan earthquake areas. *Ecol. Eng.* **2012**, *44*, 61–69.
11. Zhang, J.; Hull, V.; Huang, J.; Yang, W.; Zhou, S.; Xu, W.; Huang, Y.; Ouyang, Z.; Zhang, H.; Liu, J. Natural recovery and restoration in giant panda habitat after the Wenchuan earthquake. *For. Ecol. Manag.* **2014**, *319*, 1–9.
12. Bathurst, J.C.; Bovolo, C.I.; Cisneros, F. Modelling the effect of forest cover on shallow landslides at the river basin scale. *Ecol. Eng.* **2010**, *36*, 317–327.
13. Marston, R.A. Geomorphology and vegetation on hillslopes: Interactions, dependencies, and feedback loops. *Geomorphology* **2010**, *116*, 206–217.
14. Dahal, R.K.; Hasegawa, S.; Nonomura, A.; Yamanaka, M.; Dhakal, S.; Paudyal, P. Predictive modelling of rainfall-induced landslide hazard in the Lesser Himalaya of Nepal based on weights-of-evidence. *Geomorphology* **2008**, *102*, 496–510.
15. Kaab, A. Photogrammetry for early recognition of high mountain hazards: New techniques and applications. *Phys. Chem. Earth Part B Hydrol. Ocean. Atmos.* **2000**, *25*, 765–770.
16. Dai, F.C.; Lee, C.F. Landslide characteristics and slope instability modeling using GIS, Lantau island, Hongkong. *Geomorphology* **2002**, *42*, 213–228.
17. Gares, P.A.; Sherman, D.J.; Nordstrom, K.F. Geomorphology and natural hazards. *Geomorphology* **1994**, *10*, 1–18.
18. Zhuang, J.-Q.; Cui, P.; Ge, Y.-G.; He, Y.-P.; Liu, Y.-H.; Guo, X.-J. Probability assessment of river blocking by debris flow associated with the Wenchuan earthquake. *Int. J. Remote Sens.* **2010**, *31*, 3465–3478.
19. Qiao, G.; Lu, P.; Scaioni, M.; Xu, S.; Tong, X.; Feng, T.; Wu, H.; Chen, W.; Tian, Y.; Wang, W.; *et al.* Landslide investigation with remote sensing and sensor network: From susceptibility mapping and scaled-down simulation towards *in situ* sensor network design. *Remote Sens.* **2013**, *5*, 4319–4346.
20. Scaioni, M. Remote sensing for landslide investigations: From research into practice. *Remote Sens.* **2013**, *5*, 5488–5492.
21. Tronin, A.A. Satellite remote sensing in seismology. A review. *Remote Sens.* **2009**, *2*, 124–150.

22. Cui, X.; Gibbes, C.; Southworth, J.; Waylen, P. Using remote sensing to quantify vegetation change and ecological resilience in a semi-arid system. *Land* **2013**, *2*, 108–130.
23. Li, Z.; Jiao, Q.; Liu, L.; Tang, H.; Liu, T. Monitoring geologic hazards and vegetation recovery in the Wenchuan earthquake region using aerial photography. *ISPRS Int. J. Geo Inf.* **2014**, *3*, 368–390.
24. Tofani, V.; del Ventisette, C.; Moretti, S.; Casagli, N. Integration of remote sensing techniques for intensity zonation within a landslide area: A case study in the northern Apennines, Italy. *Remote Sens.* **2014**, *6*, 907–924.
25. Assilzadeh, H.; Levy, J.K.; Wang, X. Landslide catastrophes and disaster risk reduction: A GIS framework for landslide prevention and management. *Remote Sens.* **2010**, *2*, 2259–2273.
26. Liu, J.G.; Mason, P.J.; Yu, E.; Wu, M.-C.; Tang, C.; Huang, R.; Liu, H. GIS modelling of earthquake damage zones using satellite remote sensing and DEM data. *Geomorphology* **2012**, *139–140*, 518–535.
27. Gomes, R.; Guimarães, R.; de Carvalho, O.; Fernandes, N.; do Amaral, E. Combining spatial models for shallow landslides and debris-flows prediction. *Remote Sens.* **2013**, *5*, 2219–2237.
28. Endo, T.; Tsuruta, T. *The Effect of the Tree's Roots Upon the Shear Strength of Soil*; 1968 Annual Report of the Hokkaido Branch; Forest Experiment Station: Sapporo, Japan, 1969.
29. Swanson, F.J.; Swanston, D.N. Complex mass-movement terrains in the western cascade range, Oregon. *Rev. Eng. Geol.* **1977**, *3*, 113–124.
30. Prandini, L.; Guidiini, G.; Bottura, J.; Pançano, W.; Santos, A. Behavior of the vegetation in slope stability: A critical review. *Bull. Int. Assoc. Eng. Geol.* **1977**, *16*, 51–55.
31. Yang, X.; Chen, L. Using multi-temporal remote sensor imagery to detect earthquake-triggered landslides. *Int. J. Appl. Earth Obs. Geoinf.* **2010**, *12*, 487–495.
32. Lin, W.-T.; Chou, W.-C.; Lin, C.-Y.; Huang, P.-H.; Tsai, J.-S. Vegetation recovery monitoring and assessment at landslides caused by earthquake in central Taiwan. *For. Ecol. Manag.* **2005**, *210*, 55–66.
33. USGS. Magnitude 7.9 ShakeMap—EASTERN SICHUAN, CHINA. Available online: http://earthquake.usgs.gov/earthquakes/eqinthenews/2008/us2008ryan/#maps (accessed on 15 October 2014).
34. Dai, F.; Lee, C.; Li, J.; Xu, Z. Assessment of landslide susceptibility on the natural terrain of Lantau island, Hongkong. *Environ. Geol.* **2001**, *40*, 381–391.